RSC Advances

PAPER

View Article Online
View Journal | View Issue

Open Access Article. Published on 12 December 2023. Downloaded on 3/9/2026 5:45:25 PM.
This article is licensed under a Creative Commons Attribution-NonCommercial 3.0 Unported Licence.

Check for updates

Cite this: *RSC Adv.*, 2023, **13**, 36107

Facile preparation of carbon nitride by binary eutectic KNO_3/KCl molten salt and its photocatalytic performance evaluation†

Xiaodi Chen,‡[a] Shihang Liu,‡[a] Tian Xie,[a] Chao Zhang *[a] and Shiai Xu [ab]

Graphitic carbon nitride (g-C_3N_4) has been widely investigated and applied in photocatalysis, but it always suffers from unsatisfactory photocatalytic activity performance. In this study, a facile molten salt-assisted heat-treated g-C_3N_4 *via* binary eutectic KNO_3/KCl was successfully developed. Based on this assumption, the heat treatment temperature has been successfully lowered to 350 °C to modulate and optimize the carbon nitride structure. The obtained target photocatalysts were characterized using various characterization methods (scanning electron microscope (SEM), X-ray diffraction (XRD), X-ray photoelectron spectroscopy (XPS), ultraviolet-visible diffuse reflectance spectroscopy (UV-Vis DRS), Fourier transform infrared spectroscopy (FT-IR), photoluminescence (PL) and transient photocurrents), confirming the practicability of the proposed strategy. The presence of doped K^+ ions and the introduction of cyano groups into the main structure can strengthen the photo-induced electron–hole separation and migration ability, suppressing their recombination. Consequently, the much-enhanced photocatalytic activity of the obtained target catalyst was achieved and demonstrated through comprehensive tests such as photocatalytic degradation of organic dyes, photocatalytic degradation of pesticides, photocatalytic degradation of organic flotation reagent, and photocatalytic hydrogen production. Among these, g-CN-A-PN/PC-*T*350 exhibited the highest photocatalytic activity and the highest recycling usage stability compared with the pure sample. In addition, a possible mechanism for photocatalytic degradation of organic compounds and photocatalytic H_2 evolution was obtained based on comprehensive experimental analysis. Our finding provides a promising way for g-C_3N_4 to manipulate the photocatalytic activity simply by introducing eutectic KNO_3/KCl in the preparation process and provides a comprehensive understanding of the roles of molten salt.

Received 3rd October 2023
Accepted 7th December 2023

DOI: 10.1039/d3ra06718a

rsc.li/rsc-advances

1 Introduction

In recent years, photocatalysis has been widely used in photocatalytic decomposition of organic substances,[1–5] photocatalytic hydrogen generation,[6–8] and carbon dioxide reduction,[9–11] and has obvious privileges in solving environmental and energy challenges. Graphitic carbon nitride (g-C_3N_4), a low cost and metal-free semiconductor with suitable band gap (2.7 eV), is one of the most promising candidates that has gained considerable attention in the relevant field.[12,13] Nevertheless, its small surface area and rapid recombination of photoexcited carriers result in g-C_3N_4 with moderate photocatalytic activity.[14] To tackle these problems, various modification strategies, including element doping,[14,15] defect engineering, morphology control,[16,17] and composite construction, have been adopted.

Molten salt synthesis has been proven as a green process for preparing a wide range of nanomaterials with controllable nanostructure.[18] Generally, a molten salt can serve as a solvent for high temperature materials synthesis, a soft template for tailoring micro and mesoporosity of the materials, and a structure-directing agent in the polycondensation and deamination reactions to obtain graphitic materials.[19] For instance, Su *et al.*[20] reported a sustainable salt-induced structure remodeling method to transform amorphous PCN into crystalline KPCN by incorporating potassium ions *via* simple annealing with KCl. As a result, the obtained KPCN exhibited almost a 20-fold enhancement in photocatalytic activity for hydrogen evolution compared to the amorphous one. Liang *et al.*[21] obtained triazine-/heptazine-based g-C_3N_4 homojunctions with the cyano group defects and K^+ ions doping *via* a simple and fast one-step molten salt route. The g-C_3N_4 homojunctions demonstrated

[a]*School of Chemical Engineering, Qinghai University, Xining 810016, Qinghai, China. E-mail: zhangchaoqhu@126.com*

[b]*Shanghai Key Laboratory of Advanced Polymeric Materials, Key Laboratory for Ultrafine Materials of Ministry of Education, School of Materials Science and Engineering, East China University of Science and Technology, Shanghai 200237, China. E-mail: saxu@ecust.edu.cn*

† Electronic supplementary information (ESI) available. See DOI: https://doi.org/10.1039/d3ra06718a

‡ These authors contributed equally to this work.

© 2023 The Author(s). Published by the Royal Society of Chemistry

Open Access Article. Published on 12 December 2023. Downloaded on 3/9/2026 5:45:25 PM.
This article is licensed under a Creative Commons Attribution-NonCommercial 3.0 Unported Licence.

a 12-times higher hydrogen evolution rate than bulk ones, possibly due to the synergistic effects of K^+ ions, cyano group defects and homojunctions. Zhang *et al.*[22] prepared crystalline polymer carbon nitride using the solid-salt-assisted growth strategy with KCl as a structure-directing agent. The photocatalytic activity of CPCN in the hydrogen evolution reaction was over 22 times higher than that of pristine PCN, potentially originating from the high crystallinity of CPCN and shortened interlayer distance. Furthermore, some eutectic salt mixtures, such as LiCl and KCl,[23,24] LiBr and KBr,[25] have been explored to react with the precursors or condensation intermediates to improve the crystallinity of carbon nitride. However, most of them result in poly(triazine imides) (PTI) instead of the poly(-heptazine imides) structure, which may reduce the visible light absorption ability in photocatalysis.

As mentioned above, the commonly used inorganic salts (KCl, KBr) often have high melting points. Consequently, when used as reaction media, it is difficult to achieve a molten state and accomplish liquid phase mass transfer under relatively mild conditions. While Li containing molten salts like LiBr and LiCl can reach a molten state at lower heat treatment temperatures, enabling liquid phase mass transfer, they tend to form inactive PTI phases. Additionally, the Li containing molten salts are expensive and lead to poor thermodynamic stability and low photocatalytic activity of the target catalyst, which is unfavorable for practical applications.[26] Discovering inexpensive and low melting point non lithium molten salts holds significant value in expanding the application range of molten salt treatment for carbon nitride.

In this present work, based on the binary phase diagram, we selected KNO_3 (PN) and KCl (PC) molten salts as reaction media, and explored the performance of low melting point single potassium salt and low eutectic point composite potassium salt assisted heat treatment modified g-C_3N_4. The eutectic mixture of KNO_3/KCl exhibits a melting point of mp = 308 °C, well below the typical polymerization temperature of g-C_3N_4 (T = 550 °C), which allows at least part of the solid reactants to dissolve and facilitates improved condensation and higher structural order. The eutectic blend of KNO_3/KCl has the capability to liquefy under mild conditions, facilitating liquid-phase mass transfer, hastening the reaction progression, and lowing the supplemental heat treatment temperature of the molten salt. This presents an innovative alternative for selecting the type of molten salt. In this manner, *in situ* K^+ doping and microstructure regulation were successfully achieved by using KNO_3/KCl binary molten salt as the medium to assist in the preparation of g-C_3N_4. Subsequently, the photocatalytic performance of the obtained target catalyst was characterized through comprehensive tests such as photocatalytic degradation of organic dyes, photocatalytic degradation of pesticides, and photocatalytic hydrogen production. All these results demonstrated that the photocatalytic performance of the target catalyst was significantly improved after targeted molten salt treatment. This study provides a new approach for the design and synthesis of high photoreactive carbon nitride for versatile solar energy photocatalytic applications.

2 Experimental

2.1 Chemicals

Melamine ($C_3H_6N_6$, AR), KCl (AR), KNO_3 (AR), NH_4Cl (AR), 1,4-benzoquinone ($C_6H_4O_2$, 99%), isopropanol (C_3H_8O, AR), methanol (CH_4O, AR), and triethanolamine ($C_6H_{15}NO_3$, AR) were purchased from Sinopharm Chemical Reagent Co., Ltd. Methylene blue ($C_{16}H_{18}ClN_3S$, AR) and Mordant Red 15 dye ($C_{25}H_{21}NO_6$, AR) were purchased from Macklin. Dinotefuran ($C_7H_{14}N_4O_3$, 98%) and dodecylmorpholine ($C_{16}H_{33}NO$, 97%) were purchased from Bide Pharmatech Co., Ltd. All chemicals were purchased from chemical suppliers of analytical reagent grade without further purification.

2.2 Preparation of photocatalysts

10 g of melamine is fully ground by mortar and transferred to a semi closed alumina crucible with a lid. Under the condition of air atmosphere, the mixture is calcined at 550 °C for 4 hours at a heating rate of 5 °C min^{-1} through the programmed temperature control of muffle furnace to obtain the powder sample, which is recorded as g-CN. Besides, 10 g of melamine and 26.7 g ammonium chloride is fully ground by mortar, and the mixture is transferred to a semi closed alumina crucible. Then, the subsequent preparation process is the same as before and the obtained sample labeled as g-CN-A.

As for the typical molten salt treated sample preparation, approximately 1.5 g of g-CN-A, and a certain mass of pure KNO_3 (PN), pure KCl (PC), and KNO_3/KCl (PN/PC, mole ratio 9.53 : 1) mixed salts in a 1/10 molten salt ratio (mass ratio). After fully ground by mortar for 20 minutes and transfer them to a semi enclosed alumina crucible with a lid. Under the condition of air atmosphere, the mixture is calcined at 350 °C for 4 hours at a heating rate of 5 °C min^{-1} through the programmed temperature control of muffle furnace. After cooling to room temperature, the obtained samples were washed with deionized water and ethanol for several times, and then dried at 80 °C overnight. Finally, the obtained target catalysts were labeled g-CN-A-PN-T350, g-CN-A-PC-T350, and g-CN-A-PN/PC-T350, respectively. 1.5 g of g-CN-A without molten salt under the same heat-treating condition was labeled g-CN-A-T350 as a reference sample. The schematic diagram of the preparation process of g-CN-A-PN/PC-T350 is shown in Scheme 1. The preparation processes of the rest of the other molten salt treated samples were similar to that of g-CN-A-PN/PC-T350.

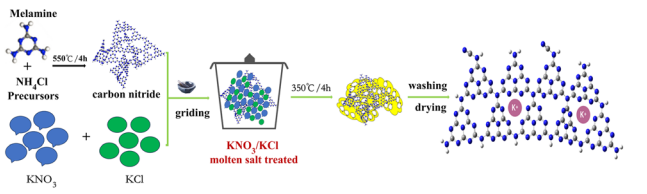

Scheme 1 Schematic diagram of the preparation process of g-CN-A-PN/PC-T350 using KNO_3/KCl molten salt.

 © 2023 The Author(s). Published by the Royal Society of Chemistry

Open Access Article. Published on 12 December 2023. Downloaded on 3/9/2026 5:45:25 PM.
This article is licensed under a Creative Commons Attribution-NonCommercial 3.0 Unported Licence.

2.3 Characterization instruments

The morphological characteristics of the samples were obtained by scanning electron microscope (ZEISS Sigma 300). The crystal structure of the sample was characterized by X-ray diffractometer (D/max 2500 PC, Rigaku), which was characterized by Cu-Kα as radiation, the scanning rate is 0.02° s^{-1}. The chemical state of the elements in the sample was characterized by multifunctional X-ray photoelectron spectroscopy (ESCALABX, Thermo Scientific). The chemical structure of the sample was characterized by Fourier transform infrared spectroscopy (IL294TGHVU, PerkinElmer) with KBr as blank. The light absorption characteristics of the sample were tested with the help of ultraviolet visible near infrared spectrophotometer (Cary 5000, Agilent) with $BaSO_4$ as the blank control. The photogenerated carrier separation ability of the sample was tested by fluorescence spectrophotometer (Cary Eclipse, Agilent) under the condition that the excitation wavelength was 330 nm and the excitation slit width 10 nm and emission slit width 5 nm.

2.4 Photocatalytic activity test

Rhodamine B (RhB), Mordant Red 15, dinotefuran and dodecylmorpholine were selected as the model organic dyes, organic pesticides and organic flotation reagent to evaluate the photocatalytic degradation performance of the molten salt prepared carbon nitride based catalysts in an aqueous solution. Typically, RhB (20 ppm), Mordant Red 15 (140 ppm), dinotefuran (10 ppm) and dodecylmorpholine (200 ppm) were used as the target pollutants. In each individual test, 100 mg of the photocatalyst was dispersed in 100 mL of the target pollutant solutions. Prior to the photocatalytic degradation test, the adsorption–desorption equilibrium was achieved by stirring the mixture in a dark environment with 30 min for RhB (20 ppm) and Mordant Red 15 (140 ppm). A 300 W xenon lamp with a 400 nm cutoff filter (illumination intensity 143.7 mW cm^{-2}) irradiated the dye solution for the purpose of degradation. As for dinotefuran (10 ppm) degradation, the adsorption–desorption equilibrium was achieved by stirring the mixture in a dark environment with 720 min and A 300 W xenon lamp with a full spectrum (illumination intensity 355.6 mW cm^{-2}) irradiated the organic pesticides solution for the purpose of degradation. Then, after a specific time interval, approximately 5 mL of the suspension was removed and centrifuged for subsequent testing. The UV-visible absorption spectra of the supernatant solution were analyzed by a UV-visible spectrometer (Shimadzu UV-2550). For the degradation of dodecylmorpholine (200 ppm), the adsorption–desorption equilibrium was achieved by stirring the mixture in a dark environment with 30 min and a 300 W xenon lamp with a full spectrum irradiated the organic pesticides solution for the purpose of degradation. Afterwards, at the specific time interval, approximately 5 mL of the suspension was removed and centrifuged for subsequent testing. The relative concentration of the supernatant solution was analyzed by a GC-MS/MS (Thermo Scientific TSQ 8000) and the processing and detection methods of samples as the same as that reported in literature report.[27] Besides, the process of adsorption capacity test of the samples is same as that of photocatalytic tests without the light source.

The photocatalytic hydrogen evolution performance of the sample was tested by the full-automatic photocatalytic system (CEL-SPH2N-S9, Ceaulight Beijing), which uses a 300 W xenon lamp as the light source. A typical catalyst loading Pt process is same as that reported in our former work.[28] The photocatalytic hydrogen evolution activity test process of the sample is carried out under the condition of cooling water at 3 °C. Firstly, 10 mg sample containing Pt, 10 mL of 10 vol% triethanolamine solution was successively added into the reactor, ultrasonic dispersion is uniform, vacuum for 20 min to remove the air in the system, turn on the light source, and photocatalytic hydrogen evolution is carried out under the auxiliary condition of cut-off filter (CUT 400 nm), the H_2 produced was qualitatively analyzed by gas chromatography with high-purity N_2 as carrier gas (GC-7920, Ceaulight Beijing). The test process of photocatalytic hydrogen evolution stability of the sample is as follows. 30 mg sample containing Pt and 30 mL of 10 vol% triethanolamine solution were successively added to the reactor, the single cycle test process is the same as the photocatalytic hydrogen evolution activity test.

2.5 Photoelectrochemical measurements

Carbon cloth was used as the working electrode, the preparation process of the working electrode and the relevant transient photocurrent test was similar to that reported in our former work too.[28] Briefly, a three-electrode system was adopted and 0.1 M Na_2SO_4 solution as the electrolyte with the xenon lamp (300 W) as the light source.

3 Results and discussion

3.1 Structure and morphology characterization of photocatalysts

The surface morphological characteristics of the catalysts were observed by using a scanning electron microscope (SEM). As shown in Fig. 1, the surface of g-CN presents a dense block like structure.[29] g-CN-A is neatly arranged in folded nanosheets. Without ammonium salt added, the surface of the g-CN-PN/PC-*T*350 sample is partially eroded by molten salt when compared to g-CN, yet the overall structure remains block-like. However, samples g-CN-A-PN-*T*350, g-CN-A-PC-*T*350, and g-CN-A-PN/PC-*T*350 are fully eroded by molten salt in comparison to g-CN-A, forming a smaller block-like structure. This phenomenon indicates that the doping of K^+ can slightly inhibit the crystal growth of the catalyst. The reduced crystal size of the catalyst aids in accelerating the transfer and separation of its own charges.[19] Additionally, it suggests that the wrinkled arrangement of g-CN-A nanosheets facilitates full contact between potassium salt and g-C_3N_4, strengthening the modification effect of molten salt. This reveals the synergistic principle between potassium salt and NH_4Cl.

As shown in Fig. S1,† energy dispersive spectrometer (EDS) was used for element mapping analysis. The characterization results indicate that samples g-CN and g-CN-A only contain

Open Access Article. Published on 12 December 2023. Downloaded on 3/9/2026 5:45:25 PM.
This article is licensed under a Creative Commons Attribution-NonCommercial 3.0 Unported Licence.

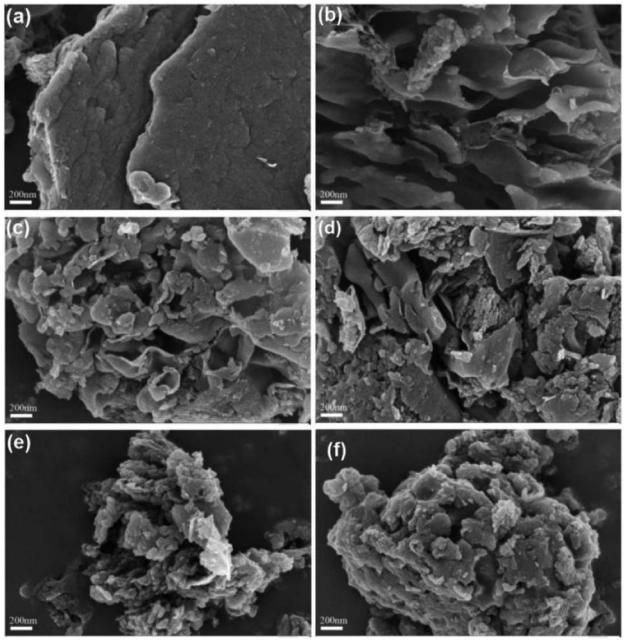

Fig. 1 SEM diagram of photocatalyst: g-CN (a), g-CN-A (b), g-CN-A-PN-*T*350 (c), g-CN-A-PC-*T*350 (d), g-CN-A-PN/PC-*T*350 (e) and g-CN-PN/PC-*T*350 (f).

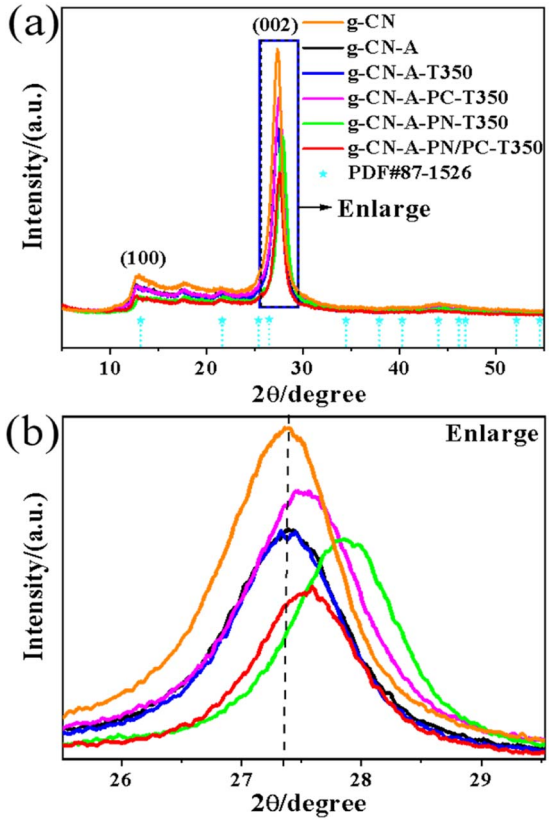

Fig. 2 XRD of the g-C_3N_4 catalyst treated by KNO_3/KCl molten salt, (a) XRD full spectrum, (b) partial enlarged view.

three elements: C, N, and O. Furthermore, Fig. S2† demonstrates that, O and K elements were also introduced in g-CN-A-PN/PC-*T*350 in addition to the existing elements C and N. It can be observed that the g-C_3N_4 modified by composite potassium salt-assisted heat treatment successfully achieved K element doping. From the surface scan characterization results, it can be deduced that K element is uniformly distributed on the surface of sample g-CN-A-PN/PC-*T*350. The g-CN sample itself does not contain chlorine element, and the chlorine element in g-CN-A evaporates and is lost after high-temperature calcination. g-CN-A-PN/PC-*T*350 sample does not introduce chlorine element again during the g-CN-A modification process, resulting all samples in the system not containing chlorine element. In addition, the sample itself does not contain Na element, too.

The X-ray diffraction (XRD) patterns of catalysts are shown in Fig. 2(a) and (b). The diffraction peak of the sample on the (100) crystal plane corresponds to the repeated filling of heptazine ring units in the g-C_3N_4 plane, while the diffraction peak on the (002) crystal plane belongs to the interlayer stacking of the g-C_3N_4 (JCPDS no. 87-1526) crystal plane.[30] All samples modified with molten salt exhibit no diffraction peak corresponding to K species,[31] indicating that during the sample synthesis process, the remaining potassium salt was completely removed after washing with deionized water and anhydrous ethanol. When compared with the g-CN sample, all samples modified with KNO_3, KCl, and KNO_3/KCl show a significant decrease in the diffraction peak intensity on the (100) and (002) crystal planes. This indicates that the introduction of potassium salt system would inhibit the growth of catalyst crystals.[31] The diminished particle size of the sample can accelerate the migration and segregation of charge carriers, which is beneficial for photocatalysis,[19] a finding agreement with the SEM characterization outcomes. Interestingly, in the presence of ammonium salts, K^+ doping can significantly shift the diffraction peaks of catalysts g-CN-A-PN-*T*350, g-CN-A-PC-*T*350, and g-CN-A-PN/PC-*T*350 towards a higher angle on the (002) crystal plane. This suggests that K^+ is embedded between g-C_3N_4 layers, significantly enhancing interlayer interactions and accelerating interlayer charge transfer, which is beneficial for photocatalysis.[32]

To determine the chemical states of C, N, O and K elements before and after the KNO_3/KCl molten salt modification, XPS measurements were performed on g-CN and the typical sample g-CN-A-PN/PC-*T*350. The typical K element signal can be observed in sample g-CN-A-PN/PC-*T*350 (Fig. 3(a) and (b)), in contrast to the pure g-CN sample (Fig. 3(a)). According to the C 1s spectrum of the sample, the two peaks observed for g-CN at binding energies of 284.41 eV and 288.4 eV correspond to the standard C–C bond[33] and N–C=N,[22] respectively. The peaks of g-CN-A-PN/PC-*T*350 at binding energies of 286.26 eV correspond to –C≡N,[22] which is consistent with the infrared characterization results. The peaks located at binding energies of 284.8 eV and 288.47 eV correspond to the C–C bond[33] and N–C=N,[22] respectively. The two peaks at binding energies of 293.28 eV and 296.09 eV correspond to the K 2p of K^+ binding energy,[22,35] differing from the binding energy of metallic potassium (294.7 eV).[22] From the N 1s spectrum of the sample, it can be observed

 © 2023 The Author(s). Published by the Royal Society of Chemistry

Open Access Article. Published on 12 December 2023. Downloaded on 3/9/2026 5:45:25 PM.
This article is licensed under a Creative Commons Attribution-NonCommercial 3.0 Unported Licence.

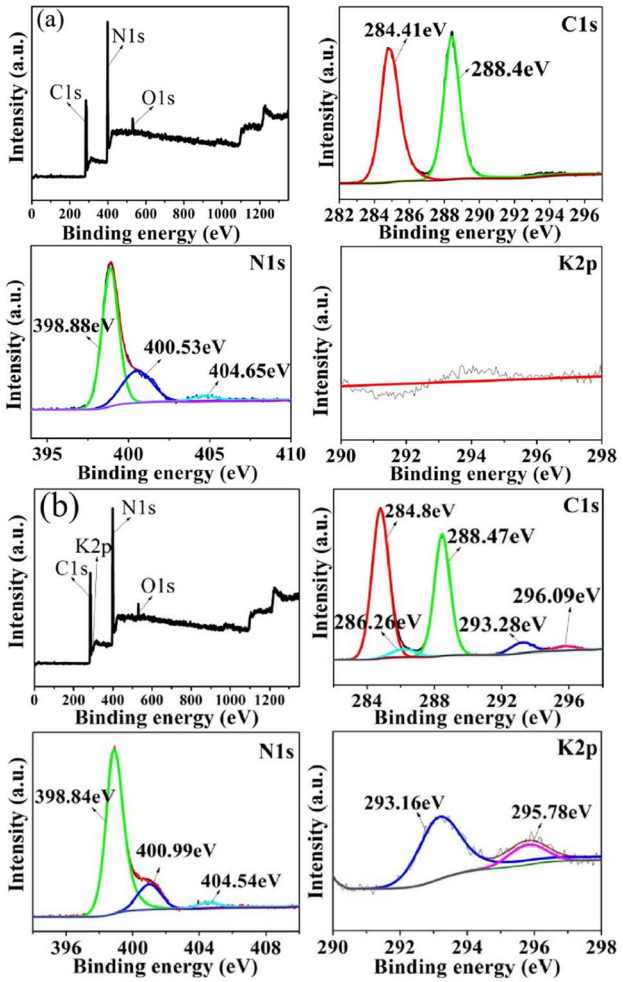

Fig. 3 XPS spectra of total spectra, C 1s spectra, N 1s spectra, and K 2p spectra of sample g-CN (a), g-CN-A-*T*-$NaNO_3$/NaCl (b).

that the peaks of g-CN at binding energies of 398.88 eV, 400.53 eV, and 404.65 eV correspond to the charging effects in C–N=C,[34] N–$(C)_3$ (ref. 35) and heterocycle,[33] respectively. The peaks observed in g-CN-A-PN/PC-*T*350, positioned at binding energies of 398.84 eV, 400.99 eV, and 404.54 eV, are corresponded to the charging effects in C–N=C,[34] N–$(C)_3$,[35] and heterocycle,[33] respectively. According to the Na 1s spectrum of the sample, there is no Na element in either g-CN or g-CN-A-PN/PC-*T*350. Regarding to the K 2p spectrum of the sample, there is no K element in g-CN. The peaks of g-CN-A-PN/PC-*T*350 at binding energies of 293.16 eV and 295.78 eV correspond to the $2p_{3/2}$ and $2p_{1/2}$ orbitals of K^+, respectively.[22]

The FT-IR spectrum of the photocatalyst is shown in Fig. 4. As observed, all samples exhibit characteristic absorption peaks of g-C_3N_4 at wave numbers 809 cm^{-1}, 1200–1700 cm^{-1}, and 3000–3500 cm^{-1}. These peaks are attributed to the bending vibration of the triazine ring, the stretching vibration of the C–N bond, and the stretching vibration of the $-NH_2$ and –NH groups that remain in g-C_3N_4 due to incomplete thermal condensation, respectively.[35,36] A new characteristic absorption peak is observed at 2176 cm^{-1} in the samples modified with KNO_3 and

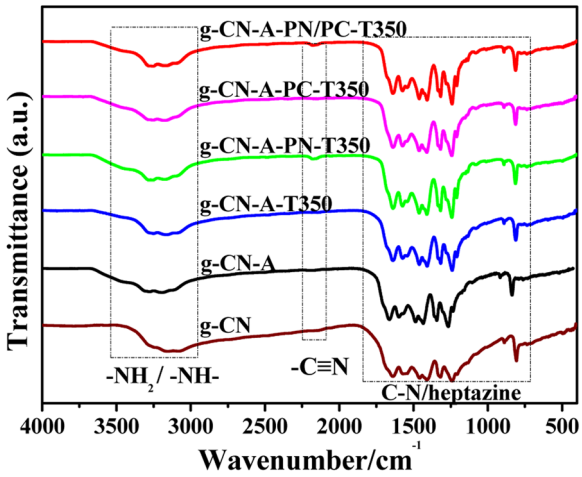

Fig. 4 FT-IR spectrum of g-C_3N_4 catalyst assisted by heat treatment in KNO_3/KCl molten salt.

KNO_3/KCl, which belongs to the asymmetric absorption peak of –C≡N.[33,34] The potential rationale behind the introduction of –C≡N resides in K^+'s ability to trigger the disintegration of the heptazine unit,[22] leading to the integration of –C≡N during the calcination process. This potent strong electron withdrawing group accelerates electron migration and enhances the photocatalytic degradation and hydrogen production performance of the corresponding catalyst. No obvious peaks are observed near 2176 cm^{-1} in the samples modified with single KCl, which indicating that the modification of the original catalyst by KCl is not obvious under the low temperature conditions of 350 °C.

3.2 Optical and photoelectrochemical properties analysis

The light-harvesting properties of the photocatalysts were characterized by using UV-Vis diffuse reflectance spectroscopy (UV-Vis DRS). As shown in Fig. 5, the absorption intensity of the g-C_3N_4 catalyst treated with molten salt was gradually increases with KCl, KNO_3 and KNO_3/KCl under the same calcined

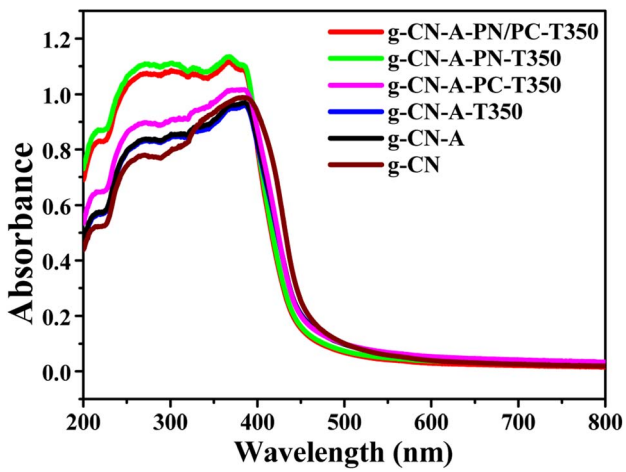

Fig. 5 UV-Vis DRS spectrum of g-C_3N_4 catalyst assisted by heat treatment in the target molten salt.

Open Access Article. Published on 12 December 2023. Downloaded on 3/9/2026 5:45:25 PM.
This article is licensed under a Creative Commons Attribution-NonCommercial 3.0 Unported Licence.

temperature. Obviously, the optical absorption strengths of the g-CN-A-PN/PC-*T*350 are significantly increased in comparison to those of the original g-CN. This kind of enhanced absorptive capacity may correspond to the introduction of cyano groups and K^+ ions in g-CN-A-PN/PC-*T*350 after KNO_3/KCl molten salt treatment. The band gap estimated from Tauc plots (shown in Fig. S3†) is 2.54 eV, 2.52 eV and 2.61 eV for g-CN, g-CN-A and g-CN-A-PN/PC-*T*350, respectively.

The XPS valence band (VB) spectrum was used to determine the band structure of samples treated with the target molten salt (Fig. S4†). The VB potentials of g-CN, g-CN-A and g-CN-A-PN/PC-*T*350 are located at +1.48, +1.57 and +2.01 eV, respectively. Then, in combination with the UV-Vis DRS results, the optical conduction band (CB) potentials of g-CN, g-CN-A and g-CN-A-PN/PC-*T*350 are situated at −1.06, −0.95 and −0.60 eV, respectively. Therefore, according to the test results, while the introduction of composite potassium salts corrects the conduction band position of the target catalyst, the conduction band positions of g-CN, g-CN-A, and g-CN-A-PN/PC-*T*350 all fulfill the requirements for photocatalytic hydrogen production. The significant change in the energy band position of the target catalyst may be caused by K^+ doping.[19]

PL is a very useful technique frequently used for research on the charge separation/recombination of photoinduced charged carriers. Generally, lower PL intensity indicates a higher separation rate of photogenerated electron–hole pairs. As shown in Fig. 6, the robust fluorescence emission peak around 455 nm observed across all samples is attributed to the recombination of their inherent electrons and holes.[37] The samples labeled as g-CN-*T*350 and g-CN-A-*T*350 denoted heat treated samples corresponding to g-CN and g-CN-A, respectively. However, simple heat treatment at 350 °C does not enhance the electron hole separation ability of g-CN and g-CN-A. When compared to g-CN, the fluorescence emission peaks of all g-C_3N_4 modified with KNO_3 and KNO_3/KCl molten salts exhibited a decreasing trend, which may be attributed to the introduction of cyanide groups strengthening the interlayer charge transfer and the doping of K^+ strengthening the interlayer charge transfer of g-CN-A-PN/PC-*T*350. The above experimental results clearly indicate that the proposed potassium salt-assisted heat treatment is the key factor in improving the electron hole separation ability of g-CN, and good electron hole separation ability is one of the important reasons for optimizing the photocatalytic performance of the target catalyst.

Transient photocurrent response is widely used to provide efficient evidence to reveal the transfer properties of the photogenerated charges of the target catalyst. As shown in Fig. 7, the photocurrent of g-CN-A-PN-*T*350 and g-CN-A-PN/PC-*T*350 is higher than that of g-CN and g-CN-A. As expected, the g-CN-A-PN/PC-*T*350 exhibited the highest photocurrent, hinting that it possesses the fastest charge transfer rate and reduces the recombination of photogenerated carriers of the target sample. The improvement in electron migration ability of g-CN-A-PN/PC-*T*350 is related to K^+ doping and the electron withdrawing group –C≡N.[38]

3.3 Evaluation of photocatalytic performance

The photocatalytic performance of the resultant target catalyst was assessed through comprehensive tests, including photocatalytic degradation of organic dyes, photocatalytic degradation of pesticides, and photocatalytic hydrogen production.

Fig. 8 illustrates the photocatalytic degradation performances of the target molten salt treated g-C_3N_4 based catalysts in the degradation of RhB dye under visible light irradiation. The degradation efficiency of RhB exhibited notable enhancement when subjected to g-CN-A-PN-*T*350 and g-CN-A-PN/PC-*T*350. The degradation rate of RhB was 60.88% (g-CN-A-PN-*T*350) and 68.76% (g-CN-A-PN/PC-*T*350) in 25 min, approximately 4.8 and 5.4 times higher than that of g-CN (12.71%). g-CN-A-PN/PC-*T*350 catalysts clearly show higher activities than that of g-CN, which is likely due to the synergistic effect caused by the introduction of cyano groups and K^+ ions in g-CN-A-PN/PC-*T*350 after KNO_3/KCl molten salt treatment.

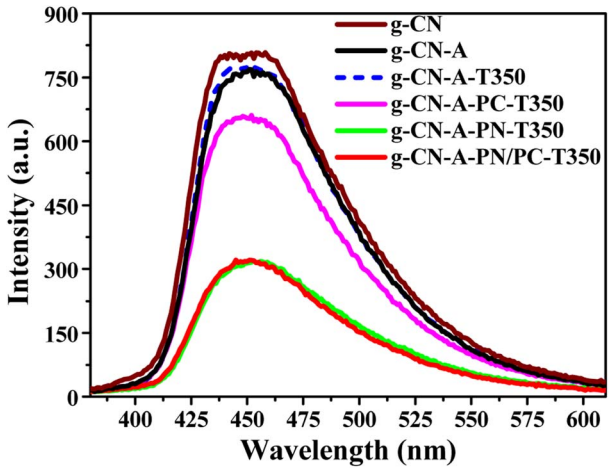

Fig. 6 PL spectrum of g-C_3N_4 catalyst assisted by heat treatment in the target molten salt (λ_{ex} = 365 nm, slit width: EX 10 nm, EM 5 nm).

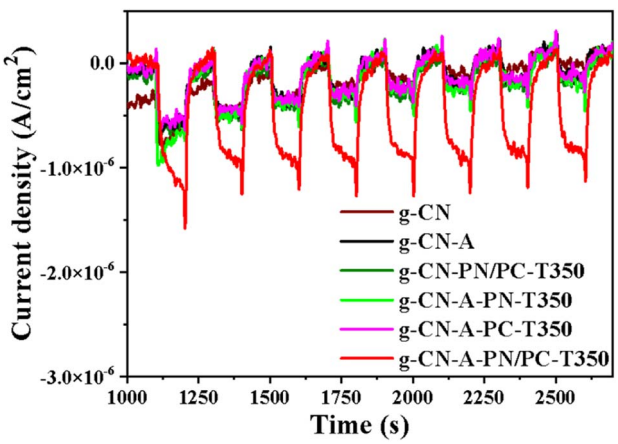

Fig. 7 Transient photocurrent responses of photocatalysts g-CN, g-CN-A, g-CN-A-PN-*T*350, g-CN-A-PC-*T*350, g-CN-A-PN/PC-*T*350 and g-CN-PN/PC-*T*350.

 © 2023 The Author(s). Published by the Royal Society of Chemistry

Open Access Article. Published on 12 December 2023. Downloaded on 3/9/2026 5:45:25 PM.
This article is licensed under a Creative Commons Attribution-NonCommercial 3.0 Unported Licence.

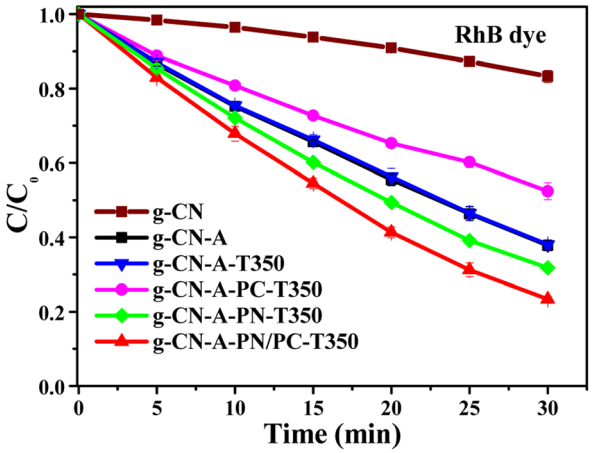

Fig. 8 Photocatalytic degradation RhB dye performance of g-C_3N_4 catalyst by heat treatment in the target molten salt.

Additionally, the photocatalytic degradation of other organic substances of g-C_3N_4 catalysts by heat treatment in the target molten salt is shown in Fig. 9. The photocatalytic degradation rate of Mordant Red 15 dye (Fig. 9(a)) was 61.84% (g-CN-A-PN/PC-*T*350) in 30 min, approximately 2.2 times higher than that of g-CN (27.80%). From Fig. 9(b), the photocatalytic degradation rate of dinotefuran pesticide was 86.92% (g-CN-A-PN/PC-*T*350) in 3 hours, approximately 3.2 times higher than that of g-CN (27.51%). As illustrated in Fig. 9(c), the photocatalytic degradation rate of dodecylmorpholine was 89.16% (g-CN-A-PN/PC-*T*350) in 120 min, which approximately 3.5 times higher than that of g-CN (25.84%). The analysis results clearly indicate that the photocatalytic degradation rates of g-CN-A-PN/PC-*T*350 for four different organic substances with varying properties are significantly improved. Besides, the adsorption capacity of the g-CN-A-PN/PC-*T*350 for different organic pollutants is listed in Table S1.† And the results show that in the sample g-CN-A-PN/PC-*T*350 has a considerable adsorption capacity the RhB dye, Mordant Red 15 dye and dodecylmorpholine. All the above outcomes indicate that this method has a universal effect on improving the performance of catalysts for the photocatalytic degradation of classic organic pollutants.

Fig. 10 shows the photocatalytic hydrogen evolution performance of g-CN, g-CN-A, g-CN-A-*T*350, g-CN-A-PC-*T*350, g-CN-A-PN-*T*350, and g-CN-A-PN/PC-*T*350, with TEOA as a sacrificial agent. As depicted in Fig. 10(a), the average hydrogen production rate of g-CN and g-CN-A within 3 h was 693.8 μmol h^{-1} g^{-1} and 1628.2 μmol h^{-1} g^{-1}, respectively. The average hydrogen production rates of the target photocatalysts g-CN-A-*T*350, g-CN-A-PC-*T*350, g-CN-A-PN-*T*350, and g-CN-A-PN/PC-*T*350 within 3 h were 1785.1 μmol h^{-1} g^{-1}, 1627.9 μmol h^{-1} g^{-1}, 2784.9 μmol h^{-1} g^{-1} and 5480.1 μmol h^{-1} g^{-1}, respectively. The g-CN-A-PN-*T*350 and g-CN-A-PN/PC-*T*350 exhibit notably higher activities, approximately 4.0 and 7.9 times higher than that of g-CN. The obtained experimental results clearly indicate that the proposed target molten salt assisted heat treatment is the key factor in improving the photocatalytic performance of the target catalyst.

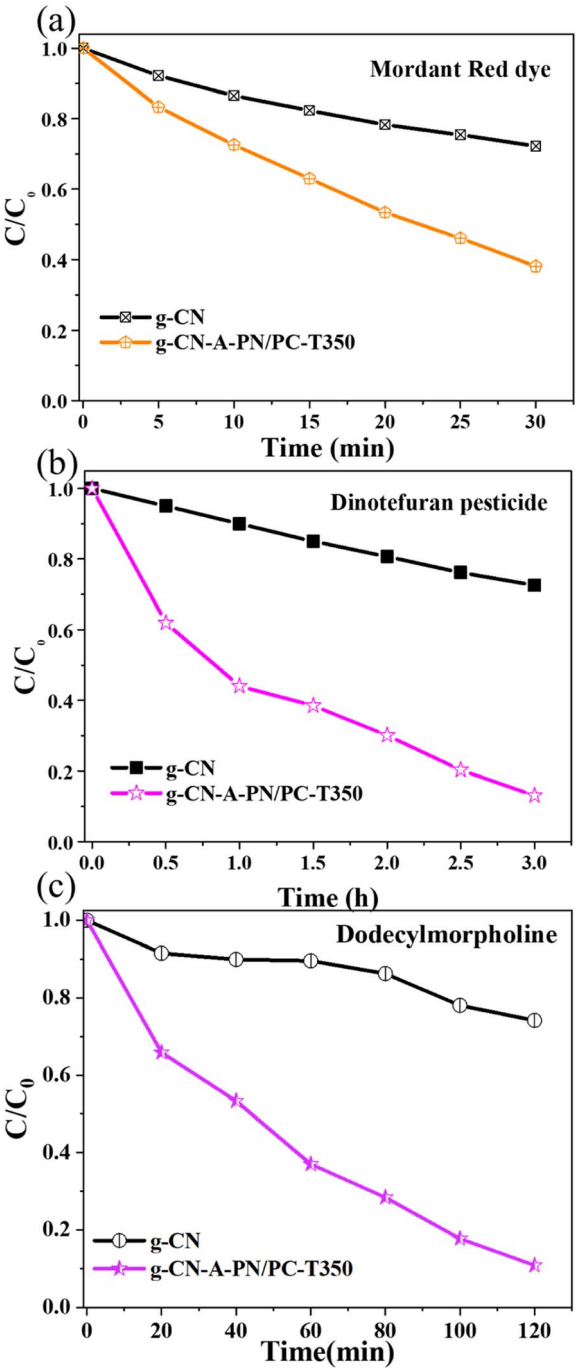

Fig. 9 Photocatalytic degradation of other organic substance of g-C_3N_4 catalyst by heat treatment in the target molten salt: (a) Mordant Red 15 dye, (b) dinotefuran pesticide, (c) dodecylmorpholine.

Since g-CN-A-PN/PC-*T*350 exhibited the highest photocatalytic hydrogen evolution performance, it was selected as the typical representative sample for studying recycling stability. As shown in Fig. 10(b), the obtained recycling results confirmed that after 7 cycles, g-CN-A-PN/PC-*T*350 still retained 99.6% of its initial photocatalytic hydrogen evolution activity, displaying outstanding stability.

Open Access Article. Published on 12 December 2023. Downloaded on 3/9/2026 5:45:25 PM.
This article is licensed under a Creative Commons Attribution-NonCommercial 3.0 Unported Licence.

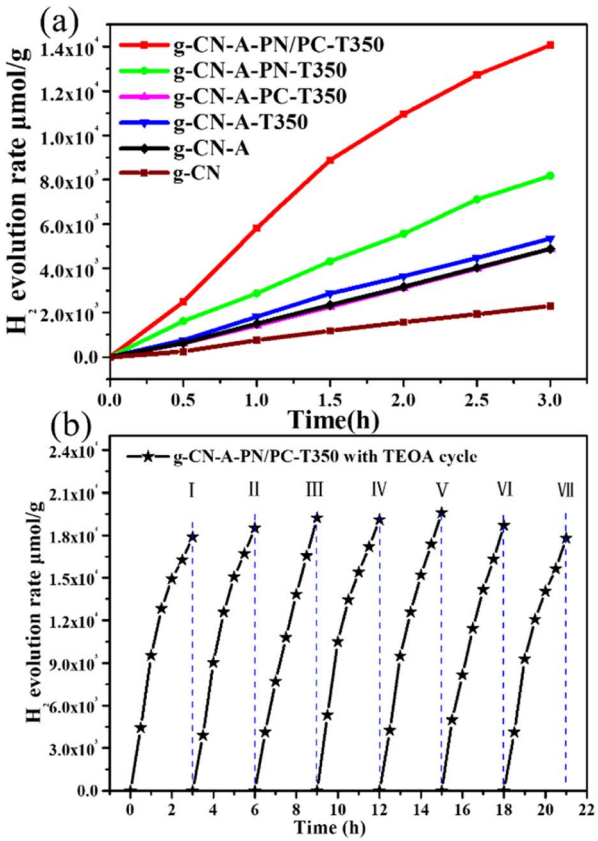

Fig. 10 The photocatalytic hydrogen performance of catalysts with TEOA as sacrificial agent under visible light ($\lambda \geq 400$ nm): (a) the photocatalytic hydrogen evolution rate of the relevant catalyst by heat treatment in the target molten salt, (b) stability test of continuous cycle hydrogen production of g-CN-A-PN/PC-*T*350.

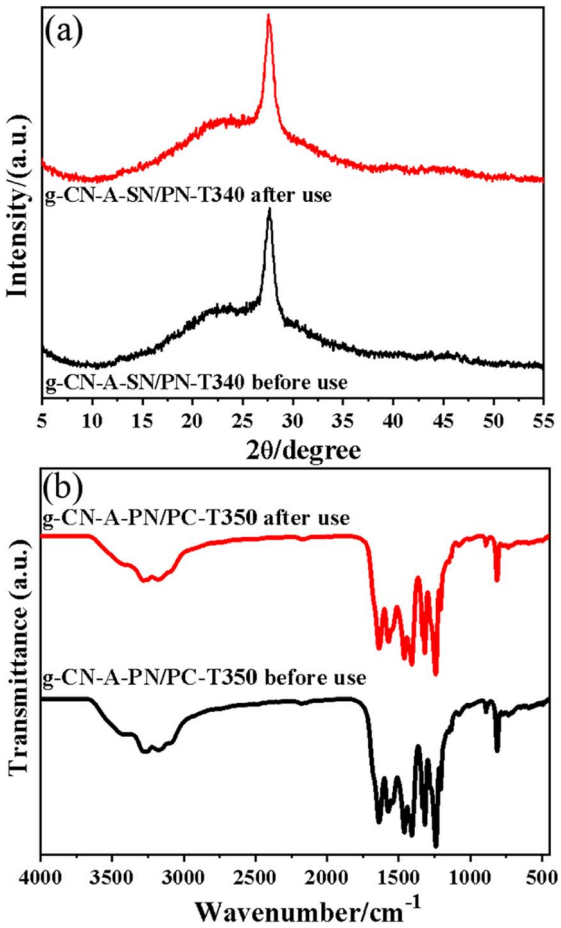

Fig. 11 (a) XRD patterns of g-CN-A-PN/PC-*T*350 before and after 7 cycles, (b) FT-IR spectra of g-CN-A-PN/PC-*T*350 before and after 7 cycles.

To further investigate the reused photocatalytic stability of g-CN-A-PN/PC-*T*350, the recycled sample after 7 cycles was collected and characterized by XRD and FT-IR (shown in Fig. 11(a) and (b)). From Fig. 11(a), the results show that before and after the recycle test, the main XRD peaks of g-CN-A-PN/PC-*T*350 show no obvious change, indicating that the main structure of the composite photocatalyst remains stable. Additionally, from the FT-IR spectrum of the samples (Fig. 11(b)), it is evident that the g-CN-A-PN/PC-*T*350 recycled sample shows no significant change compared to the original one. The above clues clearly further confirm that the g-CN-A-PN/PC-*T*350 maintains a relatively stable crystal structure.

3.4 Photocatalytic mechanism

Based on the preceding analysis, a potential mechanism for the photocatalytic degradation of organic compounds over g-CN-A-PN/PC-*T*350 is proposed and presented in Fig. 12. It is known that $^{\bullet}O_2^-$ and $^{\bullet}OH$ are the main active species for oxidizing the organic compounds. Theoretically, the redox potentials of $^{\bullet}OH/OH^-$ and $O_2/^{\bullet}O_2^-$ are +1.99 V and −0.33 V.[39] However, the VB and CB positions of g-CN are +1.48 and −1.06 eV (as determined by VB XPS test), meaning that only $^{\bullet}O_2^-$ can be formed during the photocatalytic degradation process using g-CN. After KNO_3/KCl molten salt treatment, the VB and CB positions of g-CN-A-PN/PC-*T*350 are significantly altered (+2.01 and −0.60 eV). This alteration means that the redox potential is sufficient to form both $^{\bullet}OH$ and $^{\bullet}O_2^-$, thereby leading to a considerable improvement in photocatalytic performance.

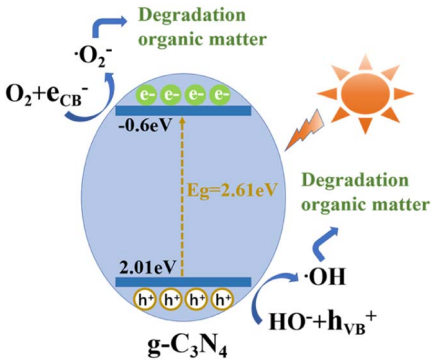

Fig. 12 The proposed mechanism for the photocatalytic degradation of organic matter using g-CN-A-PN/PC-*T*350.

 © 2023 The Author(s). Published by the Royal Society of Chemistry

Open Access Article. Published on 12 December 2023. Downloaded on 3/9/2026 5:45:25 PM.
This article is licensed under a Creative Commons Attribution-NonCommercial 3.0 Unported Licence.

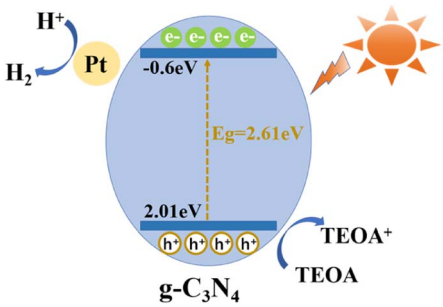

Fig. 13 The proposed mechanism for the photocatalytic evolution of H_2 over g-CN-A-PN/PC-*T*350.

Besides, a plausible mechanism for the photocatalytic evolution of H_2 over g-CN-A-PN/PC-*T*350 is proposed and depicted in Fig. 13. Under sun light irradiation, the electrons located in the VB of g-CN-A-PN/PC-*T*350 become excited to the CB, simultaneously creating holes in the VB. As mentioned before, the presence of K^+ doping and cyanide groups in g-CN-A-PN/PC-*T*350 could strengthen the photo-induced electron hole separation and migration ability, thereby suppressing their recombination. Consequently, the retained electrons migration along the g-CN-A-PN/PC-*T*350 CB can be captured by platinum deposited onto the catalyst's surface driving the photocatalytic reduction of water and subsequent hydrogen evolution reaction. The introduced TEOA as sacrificial agent may consume the holes generated in the VB to ensure the continuous progress of photocatalytic hydrogen evolution.

4 Conclusions

In conclusion, a straightforward approach involving molten salt assisted heat treatment of carbon nitride *via* the binary eutectic KNO_3/KCl has been successfully developed and the treatment temperature lowered to 350 °C. Multiple characterizations and tests have indicated that the incorporation of low eutectic composite potassium salts (KNO_3/KCl) enables the regulation of the catalyst's structure, preventing the formation of inactive phases. Additionally, controlled introduction of cyanide defect structures and *in situ* doping of K^+ elements optimizes the separation and migration of photo-induced carriers within the target catalyst. As anticipated, the prepared g-CN-A-PN/PC-*T*350 exhibits dramatically enhanced photocatalytic degradation of organic compounds and photocatalytic H_2 evolution activity compared to pure g-CN. Moreover, g-CN-A-PN/PC-*T*350 demonstrates stable catalytic activity and chemical structure during recycling usage. The present study provides a simple but very attractive way to synthesize highly-active photocatalysts by the molten salts and these target catalysts can be potentially used as an efficient, cost-effective catalyst for pollutant degradation and solar energy hydrogen production or even can be extended to other solar energy applications.

Conflicts of interest

There are no conflicts to declare.

Acknowledgements

This work is financially supported by the Project of Qinghai Science & Technology Department (Grant No. 2021-ZJ-754).

References

1 X. Zhang, K. Yue, R. Rao, J. Chen, Q. Liu, Y. Yang, F. Bi, Y. Wang, J. Xu and N. Liu, *Appl. Catal., B*, 2022, **310**, 121300.
2 Y. Yang, S. Zhao, L. Cui, F. Bi, Y. Zhang, N. Liu, Y. Wang, F. Liu, C. He and X. Zhang, *Green Energy Environ.*, 2023, **8**, 654–672.
3 H. He, Z. Luo and C. Yu, *Appl. Surf. Sci.*, 2020, **816**, 152652.
4 C. Yua, H. Heb, W. Zhou, Z. Liu and L. Wei, *Sep. Purif. Technol.*, 2019, **217**, 137–146.
5 H. He, J. Li, C. Yu and Z. Luo, *Sustainable Mater. Technol.*, 2019, **22**, e00127.
6 H. He, J. Xiao, Z. Liu, B. Yang, D. Wang, X. Peng, L. Zeng, Z. Li, L. Lei, M. Qiu and Y. Hou, *Chem. Eng. J.*, 2023, **453**, 139751.
7 J. Jia, W. Sun, Q. Zhang, X. Zhang, X. Hu, E. Liu and J. Fan, *Appl. Catal., B*, 2020, **261**, 118249.
8 J. Li, Y. Yin, E. Liu, Y. Ma, J. Wan, J. Fan and X. Hu, *J. Hazard. Mater.*, 2017, **321**, 183–192.
9 L. Xiao, R. Lin, J. Wang, C. Cui, J. Wang and Z. Li, *J. Colloid Interface Sci.*, 2018, **523**, 151–158.
10 H. Dong, X. Zhang, Y. Lu, Y. Yang, Y. Zhang, H. Tang, F. Zhang, Z. Yang, X. Sun and Y. Feng, *Appl. Catal., B*, 2020, **276**, 119173.
11 Y. Wei, L. Chen, H. Chen, L. Cai, G. Tan, Y. Qiu, Q. Xiang, G. Chen, T. Lau and M. Robert, *Angew. Chem., Int. Ed.*, 2022, **134**, 202116832.
12 Y. Zheng, L. Lin, B. Wang and X. Wang, *Angew. Chem., Int. Ed.*, 2015, **54**, 12868–12884.
13 X. Wang, K. Maeda, A. Thomas, K. Takanabe, G. Xin, J. M. Carlsson, K. Domen and M. Antonietti, *Nat. Mater.*, 2009, **8**, 76–80.
14 G. Zhang, G. Li, Z. Lan, L. Lin, A. Savateev, T. Heil, S. Zafeiratos, X. Wang and M. Antonietti, *Angew. Chem., Int. Ed.*, 2017, **129**, 13630–13634.
15 L. Jiang, X. Yuan, Y. Pan, J. Liang and G. Zeng, *Appl. Catal., B*, 2017, **217**, 388–406.
16 D. Martin, K. Qiu, S. A. Shevlin, A. D. Handoko, X. Chen, Z. Guo and J. Tang, *Angew. Chem., Int. Ed.*, 2014, **53**, 9240–9245.
17 Z. Yang, Y. Zhang and Z. Schnepp, *J. Mater. Chem.*, 2015, **3**, 14081–14092.
18 L. Tian, J. Li, F. Liang, J. Wang, S. Li, H. Zhang and S. Zhang, *Appl. Catal., B*, 2018, **225**, 307–313.
19 J. Zhao, L. Ma, H. Wang, Y. Zhao, J. Zhang and S. Hu, *Appl. Surf. Sci.*, 2015, **332**, 625–630.
20 Y. Xu, C. Qiu, X. Fan, Y. Xiao, G. Zhang, K. Yu, H. Ju, X. Ling, Y. Zhu and C. Su, *Appl. Catal., B*, 2020, **268**, 118457.
21 J. Yang, Y. Liang, K. Li, G. Yang and X. Xie, *Appl. Catal., B*, 2019, **262**, 118252.
22 Y. Xu, X. He, H. Zhong, S. David, L. Zhang and R. Wang, *Appl. Catal., B*, 2019, **246**, 349–355.

Open Access Article. Published on 12 December 2023. Downloaded on 3/9/2026 5:45:25 PM.
This article is licensed under a Creative Commons Attribution-NonCommercial 3.0 Unported Licence.

23 M. Bojdys, J. Müller, M. Antonietti and A. Thomas, *Chem.–Eur. J.*, 2008, **14**, 8177–8182.
24 A. Jorge, D. Martin, M. Dhanoa, A. Rahman, N. Makwana, J. Tang, A. Sella, F. Corà, S. Firth and J. Darr, *J. Phys. Chem. C*, 2013, **117**, 7178–7185.
25 G. Algara, N. Severin, S. Chong, T. Björkman, R. Palgrave, A. Laybourn, M. Antonietti, Y. Khimyak, A. Krasheninnikov and J. Rabe, *Angew. Chem., Int. Ed.*, 2014, **53**, 7450–7455.
26 H. Ou, L. Lin, Y. Zheng, P. Yang, Y. Fang and X. Wang, *Adv. Mater.*, 2017, **6**, 3921–3931.
27 H. Guo, *Technology of Water Treatment*, 2019, **45**, 3.
28 X. Chen, H. Bao, S. Liu, X. Liu and C. Zhang, *New J. Chem.*, 2022, **46**, 20311–20321.
29 W. Iqbal, C. Dong, M. Xing, J. Zhang and X. Tan, *Catal. Sci. Technol.*, 2017, **7**, 1726–1734.
30 C. Zhang, J. Liu, X. Huang, D. Chen and S. Xu, *ACS Omega*, 2019, **4**, 17148–17159.
31 X. Qu, S. Hu, J. Bai, P. Li, G. Lu and X. Kang, *Mater. Sci. Technol.*, 2018, **34**, 1932–1938.
32 L. Lin, H. Ou, Y. Zhang and X. Wang, *ACS Catal.*, 2016, **6**, 3921–3931.
33 Z. Shu, Y. Wang, W. Wang, J. Zhou, T. Li, X. Liu, Y. Tan and Z. Zhao, *Int. J. Hydrogen Energy*, 2019, **44**, 748–756.
34 Y. Wang, Y. Li, W. Ju, J. Wang, H. Yao, L. Zhang, J. Wang and Z. Li, *Carbon*, 2016, **102**, 477–486.
35 L. Lan, Y. Li, M. Zeng, M. Mao, L. Ren, Y. Yang, H. Liu, L. Yun and X. Zhao, *Appl. Catal., B*, 2017, **203**, 494–504.
36 Q. Wang, S. Guan and B. Li, *Catal. Sci. Technol.*, 2017, **7**, 4064–4078.
37 X. Zhang, L. Yu, C. Zhuang, T. Peng, R. Li and X. Li, *ACS Catal.*, 2014, **41**, 62–170.
38 Z. Chen, S. Lu, Q. Wu, F. He, N. Zhao, C. He and C. Shi, *Nanoscale*, 2018, **10**, 3008–3013.
39 G. Liu, P. Niu, L. C. Yin and H. Cheng, *J. Am. Chem. Soc.*, 2012, **134**, 9070–9073.

 © 2023 The Author(s). Published by the Royal Society of Chemistry